On the rigidity of four hundred Pickering-stabilised microbubbles

Nicole Anderton, Craig Stuart Carlson, Ryunosuke Matsumoto, Ri-Ichiro Shimizu, Albert Thijs Poortinga, Nobuki Kudo, Michiel Postema

Japanese Journal of Applied Physics

The Japan Society of Applied Physics

ACCEPTED MANUSCRIPT

On the rigidity of four hundred Pickering-stabilised microbubbles

To cite this article before publication: Nicole Anderton *et al* 2022 *Jpn. J. Appl. Phys.* in press https://doi.org/10.35848/1347-4065/ac4adc

Japanese Journal of Applied Physics **BRIEF NOTE**

On the rigidity of four hundred Pickering-stabilised microbubbles

Nicole Anderton[1]*, Craig S. Carlson[1,2], Ryunosuke Matsumoto[3], Ri-ichiro Shimizu[3], Albert T. Poortinga[4], Nobuki Kudo[3], and Michiel Postema[1,2]

[1]*BioMediTech, Faculty of Medicine and Health Technology, Tampere University, Korkeakoulunkatu 3, 33720 Tampere, Finland*

[2]*School of Electrical and Information Engineering, University of the Witwatersrand, Johannesburg, 1 Jan Smuts Laan, 2001 Braamfontein, South Africa*

[3]*Faculty of Information Science and Technology, Hokkaido University, Kita 14 Jo, Nishi 9 Chome, Kita-ku, Sapporo, Hokkaido 060-0814, Japan*

[4]*Department of Mechanical Engineering, Eindhoven University of Technology, De Zaale, 5600 MB Eindhoven, Netherlands*

This study explores the rigidity of Pickering-stabilised microbubbles subjected to low-amplitude ultrasound. Such microbubbles might be suitable ultrasound contrast agents. Using an adapted Rayleigh-Plesset equation, we modelled the dynamics of microbubbles with a 7.6-N m^{-1} shell stiffness under 1-MHz, 0.2-MPa sonication. Such dynamics were observed experimentally, too, using high-speed photography. The maximum expansions were agreeing with those predicted for Pickering-stabilised microbubbles. Subjecting microbubbles to multiple time-delayed pulses yielded the same result. We conclude that Pickering-stabilised microbubbles remain very stable at low acoustic amplitudes.

Pickering-stabilised bubbles have been of interest as novel ultrasound contrast agents.[1)] This study explores the rigidity of such a Pickering-stabilised ultrasound contrast agent subjected to ultrasound with a low amplitude.

Ultrasound contrast agents comprise microscopic gas bubbles typically stabilised by elastic or viscoelastic shells.[2,3)] These so-called microbubbles oscillate upon sonication.[4,5)] Administered to the blood pool by injection, ultrasound contrast agents were originally intended for diagnostic purposes through harmonic ultrasonic imaging.[6–9)] In addition to diagnostics, these agents have become of therapeutic interest, owing to the discovery of sonoporation.[10–12)] Sonoporation or sonopermeation refers to the transient permeation of cell membranes by means of ultrasound with amplitudes below the cavitation threshold, allowing for the transmembrane delivery of drugs and genes.[13)] The occurrence of sonoporation is drastically amplified by the presence of an ultrasound contrast agent.[14,15)] Even if drugs are administered separately from

*E-mail: nicole.anderton@tuni.fi

an ultrasound contrast agent, whilst a region of treatment is being sonicated, the local drug uptake in the sonicated region might increase. Such sonoporation-assisted drug delivery has been successful in the treatment of human pancreatic cancer.[16)]

It has been proposed by many groups to incorporate therapeutics directly onto or into microbubbles as to create vehicles for ultrasound-assisted drug delivery, as explained in reviews on this topic.[17,18)] Despite several attempts to manufacture such futuristic agents, however, it has not been fully understood under which acoustic conditions the carrier microbubbles are disrupted to release their payload, and what the influence of the microbubble shell is on the disruption process.

Ultrasound contrast agent microbubble disruption has been studied with high-speed photography.[19,20)] The two main mechanisms observed with ultrasound contrast agent microbubble disruption are referred to as sonic cracking and fragmentation.[20)] Sonic cracking occurs during expansion of an oscillating bubble, releasing the gaseous bubble contents through one or more pores or cracks in the shell. It has been exclusively observed with ultrasound contrast agent microbubbles with inflexible shells of thickness greater than 100 nm. Fragmentation occurs when the bubble is contracting. Fragmentation can result from a surplus of kinetic energy over surface energy during contraction or from asymmetric collapse, also known as jetting. It has been exclusively observed with ultrasound contrast agent microbubbles with surfactant shells of a few nanometers thickness. Both sonic cracking and fragmentation results in the formation of free gas bubbles.[20)] Such free gas microbubbles dissolve within milliseconds.[3)]

Instead of being surrounded by a physical shell, a microbubble may have been stabilised by adsorbing colloidal particles at the gas–liquid interface. This process is called Pickering stabilising.[21)] Pickering-stabilised microbubbles are rigid at ambient hydrostatic pressures.[22)] Despite this rigidity, shrinking of Pickering-stabilised microbubbles has been occasionally observed during single-pulse sonication.[1)] Microbubble gas dissolution could be ruled out here, as this is very slow relative to the oscillation times.[3)] A hypothetical explanation might be that the stabilised shell rearranged itself during sonication to take up less surface area.

Having also observed disruption of a Pickering-stabilised antibubble at a high acoustic amplitude,[23)] we hypothesised that ultrasound might influence the shell rigidity. The present study focussed on the rigidity of Pickering-stabilised microbubbles at a low acoustic amplitude. We theoretically modelled and experimentally observed the dynamics of Pickering-stabilised microbubbles with special attention to radial excursions during the first oscillation cycle.

The radial oscillatory motion of bubbles is typically described by a type of Rayleigh-Plesset equation. Over the past 100 years, Rayleigh-Plesset equations have been modified to

incorporate terms to account for the viscosity of the surrounding liquid, dynamic thermal conditions, and the presence of an encapsulating shell, just to name a few.[24–27] As we concentrate on disruption in the paper, we are less interested in the accuracy of the model beyond the first two cycles. Therefore, we may use a rather simple model, whose derivation we presented earlier,[28] whilst ignoring any solid potentially present inside the microbubble and by adding damping terms and a shell stiffness parameter.[25,29]

For an encapsulated microbubble driven by an acoustic wave, the fundamental equation is then given by

$$\begin{aligned} R\ddot{R} + \tfrac{3}{2}\dot{R}^2 = \frac{1}{\rho}\Bigg[&\left(p_0 - p_\mathrm{v} + \frac{2\sigma}{R_0}\right)\left(\frac{R_0}{R}\right)^{3\gamma} \\ &+ p_\mathrm{v} - \frac{2\sigma}{R} - 2\chi\left(\frac{1}{R_0} - \frac{1}{R}\right) \\ &- \frac{4\eta\dot{R}}{R} - \delta\omega\rho R\dot{R} - p_0 - p(t)\Bigg], \end{aligned} \tag{1}$$

where $p(t)$ is the time-dependent acoustic driving function, p_0 is the ambient pressure, p_v is the vapour pressure, R is the instantaneous radius, R_0 is the initial radius, γ is the ratio of specific heats, δ is the damping coefficient, η is the liquid viscosity, ρ is the liquid density, σ is the surface tension, χ is the shell stiffness, and ω is the angular driving frequency.

As the viscous damping has been directly included in (1), δ only comprises the damping owing to reradiation and the thermal damping, yielding $\delta \approx kR + \frac{3}{5}(\gamma - 1)$, where $k = \frac{\omega}{c}$ is the wave number, in which c is the speed of sound.

During expansion, a Pickering-stabilised interface is regarded frictionless and of constant surface tension. The latter assumption has been confirmed experimentally.[30] As fragmentation typically occurs during the onset of collapse, we may ignore any effects typical for contraction, provided that simulations after the first collapse phase are disregarded.

On the time interval $[-10\,\mu\mathrm{s}, 10\mu\mathrm{s}]$, a driving function was defined by

$$p(t) = \begin{cases} A\sin\omega t & \forall \quad t \in [0\,\mu\mathrm{s}, 3\,\mu\mathrm{s}] \\ 0 & \forall \quad t \notin [0\,\mu\mathrm{s}, 3\,\mu\mathrm{s}] \end{cases}, \tag{2}$$

where the acoustic amplitude $A = 1.0\,\mathrm{MPa}$ and $\omega = 2\pi \times 10^6\,\mathrm{rad\,s^{-1}}$. This driving function corresponded to a three-cycle pulse of 1-MHz centre frequency.

Numerical solutions of (1) were computed using the `ode45` differential equation solver of MATLAB® (The MathWorks, Inc., Natick, MA, USA), assuming the following parameters constant: $k = 4.23\times10^3\,\mathrm{m^{-1}}$, $p_0 = 101\,\mathrm{kPa}$, $p_\mathrm{v} = 2.33\,\mathrm{kPa}$, $\gamma = 1.4$, $\eta = 1.00\,\mathrm{mPa\,s}$, $\rho = 998\,\mathrm{kg\,m^{-3}}$, and $\sigma = 0.072\,\mathrm{N\,m^{-1}}$. For free or released gas microbubbles χ must be zero.

The $R(t)$ curves computed were automatically cut off after the first oscillation cycle, after which the maximum expansion radius $R_{\max}$ was determined. The combined outcome of the simulations were two curves $R_{\max}(R_0)$, one for Pickering-stabilised microbubbles, the other for free gas microbubbles. These were to be compared with experimental footage of microbubble expansion. A small subset of these data has been presented as controls in a different study.[31)]

The Pickering-stabilised air-comprising microbubbles studied had been produced as previously published,[32)] without core material present. For Pickering-stabilisation, Aerosil® R 972 hydrophobised silica particles (Evonik Industries AG, Essen, Germany) had been added, with diameters less than 30 nm. Microbubble populations stabilised with these hydrophobised silica particles had been studied as controls at low acoustic amplitudes.[33)] These populations had been measured to have a mean radius of 3 μm. Panfilova et al. estimated the bulk resonance frequency near 1 MHz.[33)]

A quantity of 5 mg of freeze-dried material was deposited into a FALCON® 15 mL High-Clarity Polypropylene Conical Tube (Corning Science México S.A. de C.V., Reynosa, Tamaulipas, Mexico), after which 5.0 mL of 049-16787 Distilled Water (FUJIFILM Wako Pure Chemical Corporation, Chuo-Ku, Osaka, Japan) was added. The emulsion was shaken gently by hand for 1 minute. For each experiment, 0.2 mL was pipetted into the observation chamber of a high-speed observation system.[34)]

The experimental procedure for collecting high-speed video footage of Pickering-stabilised microbubbles under high-amplitude sonication was almost identical to the procedure used to collect footage from antibubbles.[31)] The observation chamber was placed under an Eclipse Ti inverted microscope (Nikon Corporation, Minato-ku, Tokyo, Japan) with a Plan Apo LWD 40×WI (N.A. 0.8) objective lens. Attached to the microscope was an HPV-X2 high-speed camera (Shimadzu, Nakagyo-ku, Kyoto, Japan), operating at frame rates equal to ten million frames per second.[35)] The exposure time corresponded to 0.10 μs per frame. Each frame corresponded to a 145×91-μm^2 area.

During each video recording, the observation chamber was subjected to one ultrasound pulse from a laboratory-assembled focussed single-element transducer.[34,35)] Each pulse had a centre frequency of 1.0 MHz. The voltage amplitude of the pulse was 1 V. In a running wave field, this voltage corresponded to a peak-negative acoustic pressures of 0.20 MPa. The transmitted pulse started with the compression phase. The signal fed into the transducer was generated by an AFG320 arbitrary function generator (Sony-Tektronix, Shinagawa-ku, Tokyo, Japan) and amplified by a UOD-WB-1000 wide-band power amplifier (TOKIN Corporation, Shiroishi, Miyagi, Japan).

A total number of 400 microbubbles subjected to 1-V pulses was analysed. Only events were selected in which the distances between microbubbles were much greater than the maximum excursions. Each video sequence consisted of 256 frames. The video sequences were stored on a personal computer and processed offline using a method previously published.[28] The first oscillation cycle was taken into account to determine $R_{\max}$. The outcome of the processing were $R(t)$ curves for all 400 microbubbles, and their respective $R_{\max}$ values.

The experiments done served to determine the shell stiffness of the Pickering-stabilised bubbles. The estimated value for χ was obtained as follows. Excursion amplitudes were taken from bubbles sonicated at a 1-V pulse amplitude. A least-squares fit through the measured excursion amplitudes yielded $R_{\max} = 1.082R_0$. Iterating through (1) using 0.1-N m^{-1} increments for $\chi \in [1.0, 20.0]$ N m^{-1}, $R_{\max}(R_0)$ curves were created through which $y = ax$ least-squares fits were computed. The fit with a closest to 1.082 corresponded to $\chi = 7.6$ N m^{-1}. Hence, the stiffness determined for the Pickering-stabilised shell is approximately equal to that of a rigid albumin-shelled ultrasound contrast agent.[36]

We performed a stability analysis by subjecting six individual bubbles to three consecutive 1-minute delayed pulses. The respective bubble dynamics were observed to be the same for each pulse, as illustrated by the event shown in Figure 1. It was observed that microbubbles Pickering-stabilised with hydrophobised silica were not disrupted at these low acoustic amplitudes.

The Pickering-stabilised microbubbles were observed to contract and expand subsequently. As an example, Figure 2 shows the radial dynamics during the first oscillation cycle of a Pickering-stabilised microbubble of 4.6-μm initial radius, measured from high-speed videos. In addition, $R(t)$ curves simulated for an encapsulated microbubble and for a free microbubble have been included. The measured data correspond to the first cycle of the simulated $R(t)$ curve of a microbubble with shell stiffness $\chi = 7.6$ N m^{-1} and clearly do not correspond to the much greater expansion of a free microbubble.

The Pickering-stabilised microbubble whose dynamics are shown in Figure 2 did not appear to have undergone gas release. From this observation, we deduct, that stabilising particles must have been present on the interface during expansion. As the experimental data matched the $R(t)$ curves, we conclude that the disruption did not take place during these first oscillation cycles.

By definition, the initial internal pressure, $p_0 - p_v + \frac{2\sigma}{R_0}$, cannot be lower than the hydrostatic pressure. Hence, the assumption that sonic cracking should have resulted in gas escape observations was justified.

Figure 3 shows an overview of R_{max} as a function of R_0. More than 90% of the microbubble excursions fitted the simulated $R_{max}(R_0)$ curve at $\chi = 7.6\,\mathrm{N\,m^{-1}}$. Consequently, the shell stiffness computed is a good representation for the stiffness of the Pickering-stabilised shell.

Follow-up studies will need to answer, whether ultrasound-assisted Pickering-stabilised shell disruption can be predicted at high acoustic amplitudes.

Following equations (8)–(10) by Doinikov et al.,[26] it was found that at 1-MHz sonication the resonant radius of Pickering-stabilised bubbles must be 9.6 μm, for $\chi = 7.6\,\mathrm{N\,m^{-1}}$. Microbubbles of initial radii greater than 5.0 μm were excluded from this study, as they are not of clinical relevance.

In summary, the maximum radial expansions observed were agreeing with the maxima predicted by the model of Pickering-stabilised microbubbles. These observations support the previous assumption that the rigidity of Pickering-stabilised shells is high. Gas release from these disrupted microbubbles was not observed, indicating that the particle structuring remained on the interface during radial oscillation. Subjecting microbubbles to multiple time-delayed pulses yielded the same result. We conclude that Pickering-stabilised microbubbles remain very rigid at low acoustic amplitudes.

Acknowledgements

This work was supported by JSPS KAKENHI, Grant Numbers JP17H00864 and JP20H04542, by the National Research Foundation of South Africa, Grant Number 127102, and by the Academy of Finland, Grant Number 340026.

References

1) N. Anderton, C. S. Carlson, R. Matsumoto, R. Shimizu, A. T. Poortinga, N. Kudo, and M. Postema, Proc. 42nd UltraSonic Electronics Symp., 2021, 2E4-4.
2) M. Chan and K. Soetanto, Jpn. J. Appl. Phys. **37**, 3078 (1998).
3) K. Yoshida, M. Ebata, C. Kaneko, Y. Zhang, Y. Shibata, K. Saito, T. Toyota, H. Hayashi, and T. Yamaguchi, Jpn. J. Appl. Phys. **60**, SDDE10 (2021).
4) Y. Yamakoshi and M. Koganezawa, Jpn. J. Appl. Phys. **44**, 4583 (2005).
5) K. Kawabata, R. Asami, T. Azuma, and S. Umemura, Jpn. J. Appl. Phys. **49**, 9 (2010).
6) S. Tano, N. Ueno, T. Tomiyama, and K. Kimura, Clin. Radiol. **52**, 41 (1997).
7) K. Kawabata, N. Sugita, H. Yoshikawa, T. Azuma, and S. Umemura, Jpn. J. Appl. Phys. **44**, 4548 (2005).
8) H. Yoshikawa, T. Azuma, K. Sasaki, K. Kawabata, and S. Umemura, Jpn. J. Appl. Phys. **45**, 4754 (2006).
9) M. Tanabe, K. Okubo, N. Tagawa, and T. Moriya, Jpn. J. Appl. Phys. **47**, 4149 (2008).
10) K. Tachibana and S. Tachibana, Jpn. J. Appl. Phys. **38**, 3014 (1999).
11) L. B. Feril Jr., T. Kondo, Y. Tabuchi, R. Ogawa, Q.-L. Zhao, T. Nozaki, T. Yoshida, N. Kudo, and K. Tachibana, Jpn. J. Appl. Phys. **46**, 4435 (2007).
12) Y. Yamakoshi, T. Miwa, N. Yoshizawa, H. Inoguchi, and D. Zhang, Jpn. J. Appl. Phys. **49**, 07HF17 (2010).
13) S. M. Nejad, H. Hosseini, H. Akiyama, and K. Tachibana, Theranostics **6**, 446 (2016).
14) K. Okada, N. Kudo, K. Niwa, and K. Yamamoto, J. Med. Ultrasonics **32**, 3 (2005).
15) N. Kudo, K. Okada, and K. Yamamoto, Biophys. J. **96**, 4866 (2009).
16) G. Dimcevski, S. Kotopoulis, T. Bjånes, D. Hoem, J. Schjøtt, B. T. Gjertsen, M. Biermann, A. Molven, H. Sorbye, E. Mc Cormack, M. Postema, and O. H. Gilja, J. Control. Release **243**, 172 (2016).
17) M. Postema and O. H. Gilja, Curr. Pharm. Biotechnol. **8**, 355 (2007).
18) J. Rich, Z. Tian, and T. J. Huang, Adv. Mater. Technol. 2100885 (2021).
19) N. Kudo, T. Miyaoka, K. Kuribayashi, and K. Yamamoto, J. Acoust. Soc. Am. **108**, 2547 (2000).
20) M. Postema, A. van Wamel, C. T. Lancée, and N. de Jong, Ultrasound Med. Biol. **30**, 827 (2004).
21) A. T. Poortinga, Langmuir **27**, 2138 (2011).
22) Z. Du, M. P. Bilbao-Montoya, B. P. Binks, E. Dickinson, R. Ettelaie, and B. S. Murray,

Langmuir **19**, 3106 (2003).

23) N. Anderton, C. S. Carlson, N. Kudo, A. T. Poortinga, and M. Postema, Jpn. J. Appl. Phys. **60**, 128001 (2021).
24) I. C. Macedo and W.-J. Yang, Jpn. J. Appl. Phys. **11**, 1124 (1972).
25) N. de Jong, R. Cornet, and C. T. Lancée, Ultrasonics **32**, 447 (1994).
26) A. A. Doinikov, J. F. Haac, and P. A. Dayton, Ultrasonics **49**, 263 (2009).
27) W. Soliman, T. Nakano, N. Takada, and K. Sasaki, Jpn. J. Appl. Phys. **49**, 116202 (2010).
28) C. S. Carlson, R. Matsumoto, K. Fushino, M. Shinzato, N. Kudo, and M. Postema, Jpn. J. Appl. Phys. **60**, SDDA06 (2021).
29) P. J. A. Frinking and N. de Jong, Ultrasound Med. Biol. **24**, 523 (1998).
30) H. Wang and P. R. Brito-Parada, J. Colloid Interface Sci. **587**, 14 (2021).
31) N. Kudo, R. Uzbekov, R. Matsumoto, R. Shimizu, C. S. Carlson, N. Anderton, A. Deroubaix, C. Penny, A. T. Poortinga, D. M. Rubin, A. Bouakaz, and M. Postema, Jpn. J. Appl. Phys. **59**, SKKE02 (2020).
32) A. T. Poortinga, Colloids Surf. A: Physicochem. Eng. Aspects **419**, 15 (2013).
33) A. Panfilova, P. Chen, R. J. G. van Sloun, H. Wijkstra, M. Postema, A. T. Poortinga, and M. Mischi, Med. Phys. **48**, 6765 (2021).
34) N. Kudo, IEEE Trans. Ultrason. Ferroelect. Freq. Control **64**, 273 (2017).
35) S. Imai and N. Kudo, Proc. IEEE Int. Ultrason. Symp., 2018, p. 184.
36) N. de Jong, PhD Thesis, Erasmus Univ. Rotterdam, 1993.

List of figures

Fig. 1. Radius measured as a function of time for a Pickering-stabilised microbubble of initial radius $R_0 = 4.9\,\mu$m, subjected to three consecutive ultrasound pulses. The response owing to the first pulse is shown in black, to the second pulse in dark purple, and to the third pulse in bottle green.

Fig. 2. Radius measured as a function of time for a Pickering-stabilised microbubble (○), simulated $R(t)$ curves of a free (—) and a shell-stabilised (**—**) microbubble of $R_0 = 4.6\,\mu$m, and inlays extracted from high-speed video footage. Each inlay corresponds to a 15-μm diameter.

Fig. 3. Scatter plot of maximum microbubble expansion measured as a function of initial radius (○), overlain with simulated $R_{\max}(R_0)$ curves of free (—) and Pickering-stabilised (**—**) microbubbles.

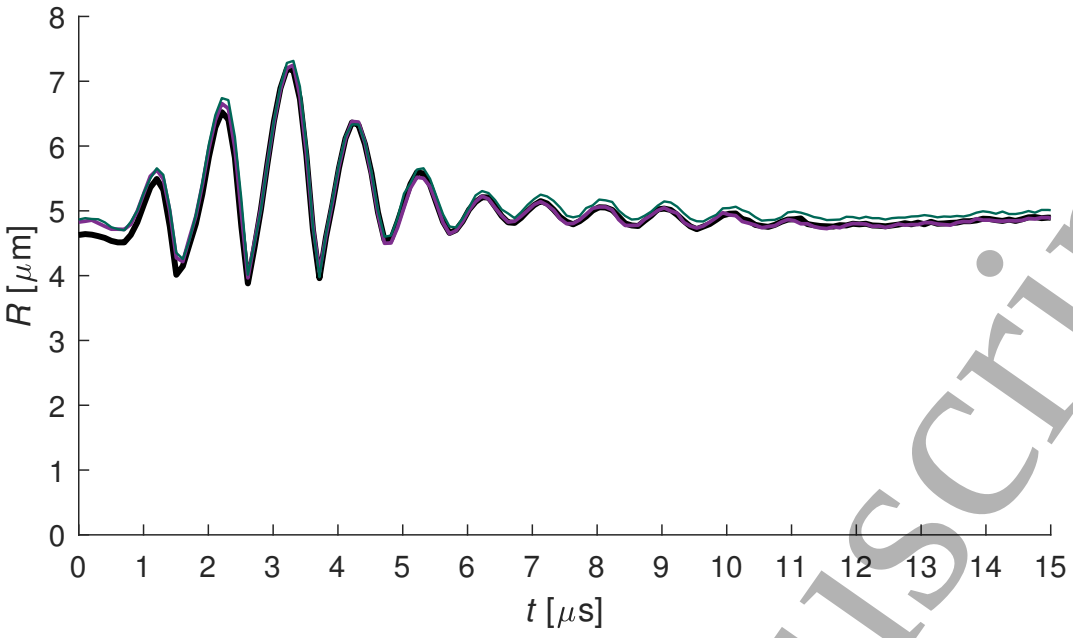

Fig. 1. Radius measured as a function of time for a Pickering-stabilised microbubble of initial radius $R_0 = 4.9\ \mu$m, subjected to three consecutive ultrasound pulses. The response owing to the first pulse is shown in black, to the second pulse in dark purple, and to the third pulse in bottle green.

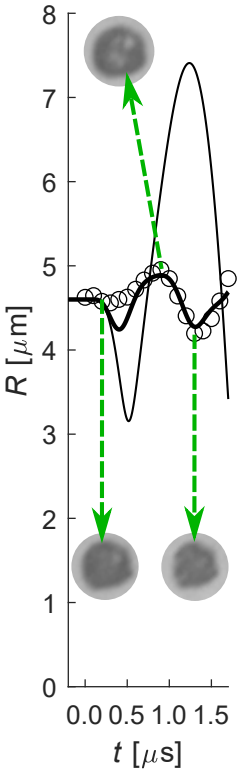

Fig. 2. Radius measured as a function of time for a Pickering-stabilised microbubble (○), simulated $R(t)$ curves of a free (—) and a shell-stabilised (**—**) microbubble of $R_0 = 4.6$ μm, and inlays extracted from high-speed video footage. Each inlay corresponds to a 15-μm diameter.

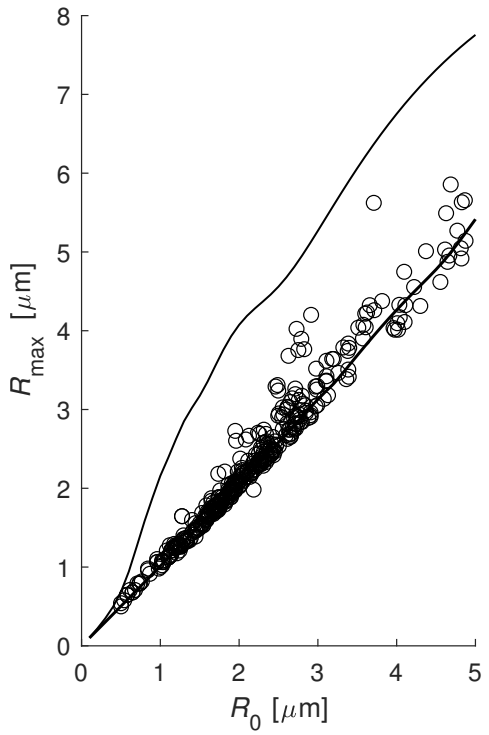

Fig. 3. Scatter plot of maximum microbubble expansion measured as a function of initial radius (○), overlain with simulated $R_{max}(R_0)$ curves of free (—) and Pickering-stabilised (—) microbubbles.